

Experimental study of the NaCl–H₂O system up to 28 GPa: Implications for ice-rich planetary bodies

Mark R. Frank^{a,*}, Claire E. Runge^{b,1}, Henry P. Scott^c, Steven J. Maglio^a,
Jessica Olson^a, Vitali B. Prakapenka^d, Guoyin Shen^{d,2}

^a Department of Geology and Environmental Geosciences, Northern Illinois University, DeKalb, IL 60115, United States

^b Department of Geology, The College of William and Mary, Williamsburg, VA 23187, United States

^c Department of Physics and Astronomy, Indiana University South Bend, South Bend, IN 46634, United States

^d Center for Advanced Radiation Sources, University of Chicago, Argonne, IL 60439, United States

Received 6 September 2005; received in revised form 11 November 2005; accepted 2 December 2005

Abstract

Recent studies have hypothesized that high-pressure H₂O polymorphs, specifically Ice VI and Ice VII, make up a significant portion of the interiors of select outer planets and their moons; most notably the Galilean satellites, Saturn's Titan and possibly Neptune's moon Triton as well as potential H₂O-rich extra-solar bodies. Several of these bodies have been conjectured to contain subsurface salty H₂O waters; therefore, any potential ice phases in the interior of these satellites could have interacted extensively with the salty oceans. Raman spectroscopy and synchrotron radiation have been used previously to study the bonding structure and unit cell parameters of pure Ice VII. However, no data exist on the effect of salts on the unit cell parameters and volume of solid H₂O at high pressure. To obtain pertinent data for use in planetary physics, it is important to understand the effect of impurities on H₂O at high pressure. The NaCl–H₂O system was chosen as a first order approximation of H₂O-rich planetary bodies. The unit cell parameters and OH stretching frequencies of Ice VII formed from 5 and 10 wt.% NaCl–H₂O solutions were studied in detail up to 27 GPa at 298 K by using a diamond anvil cell, synchrotron X-ray radiation and Raman spectroscopy. The data indicate that, over the range in pressure and temperature of this study, the maximum solubility of solutes in Ice VII was not pressure dependent. Our data suggest that the maximum concentration of NaCl that can be incorporated into Ice VII at 298 K is 7.5 ± 2.5 wt.% (or 2.4 ± 0.8 mol% NaCl). Ice VII formed from a 5 wt.% NaCl–H₂O solution has a density that is up to 5% greater at any given pressure relative to the density of Ice VII formed from pure H₂O. Additionally, the bulk modulus, 26.2 ± 1.4 GPa, was found to be approximately 10–20% greater relative to Ice VII formed from pure H₂O. Relative OH stretching frequency shifts from Ice VII formed from the NaCl–H₂O solutions were compared to Ice VII formed from pure H₂O. Ice VII formed from a 5 wt.% NaCl–H₂O solution shows a systematic increase of approximately 15 rel cm^{-1} in the OH stretching frequency relative to pure Ice VII for any given pressure. We hypothesize that the incorporation of Na⁺ and Cl⁻ into the body centered cubic structure of Ice VII results in systematic variations in the intensive thermodynamic properties of Ice VII formed from low salinity solutions. These new data will provide an improved first order approximation of high-pressure H₂O phases found within H₂O-rich bodies and should be used to model the density profiles of H₂O-rich bodies.

© 2005 Elsevier B.V. All rights reserved.

Keywords: Icy satellites; NaCl–H₂O; High pressure; Impurities; Subsurface oceans

* Corresponding author. Tel.: +1 815 753 8395; fax: +1 815 753 1945.

E-mail address: mfrank@niu.edu (M.R. Frank).

¹ Present address: Department of Geosciences, Princeton University, Guyot Hall, Princeton, NJ 08544, United States.

² Present address: HPCAT, Carnegie Institution of Washington, Advanced Photon Source, Argonne National Laboratory, Argonne, IL 60439, United States.

1. Introduction

The last 30 years have seen tremendous advances in our understanding of the internal structure and chemical stratification of the icy bodies. The initial models of the icy satellites were derived mainly from cosmochemical and observational data (e.g., *Consolmagno and Lewis, 1976*) with a bias towards explaining solar system evolution and formation. The Voyager, Galileo and Cassini-Huygens missions have supplied data detailing the outer Planets and their moons, most notably the Galilean satellites and Saturn's Titan, suggesting numerous geologic processes were and are active (*Anderson et al., 1996; Carlson et al., 1996; Kivelson et al., 1996; Schubert et al., 1996; Khurana et al., 1998; McCord et al., 1998; Brown and Calvin, 2000; Greeley et al., 2000; Greeley et al., 2000b; Zimmer et al., 2000; Anderson et al., 2001; McCord et al., 2001; Schenk et al., 2001; Head et al., 2002*). Further, these data have been used in the construction of cosmochemical and physical models of the interiors of these planetary bodies (e.g., *Mueller and McKinnon, 1988; Nellis et al., 1988; Hubbard and Marley, 1989; Anderson et al., 1996; Anderson et al., 1997; Kivelson et al., 1996; Schubert et al., 1996; Khurana et al., 1998; Zimmer et al., 2000; McCord et al., 2001; Kivelson et al., 2002; Scott et al., 2002; Sohl et al., 2002; Spohn and Schubert, 2003*). Some of these studies have hypothesized that high-pressure H₂O polymorphs, specifically Ice VI and Ice VII, may make up a significant portion of these bodies. Ice VI belongs to the tetragonal crystal system and is stable from approximately 1–2.2 GPa at 298 K. Ice VII is stable from 2.2 to approximately 62 GPa at 298 K and has a body centered cubic arrangement consisting of two interpenetrating cubic ice lattices with no connecting hydrogen bonds between lattices; the hydrogen bonding is disordered.

Recent studies have hypothesized that several of Jupiter's satellites have subsurface salty H₂O waters (*Kargel, 1991; Kargel et al., 1991; Kargel, 1992; Khurana et al., 1998; Zimmer et al., 2000; Kivelson et al., 2000*). Additionally, the melting curve of Ice VII (*Datchi et al., 2000*) illustrates that this polymorph of H₂O is stable up to approximately 325 °C at pressures equivalent to the core pressures of Ganymede, Callisto and Titan. This “warm” ice could have interacted extensively with the subsurface oceans, other “ice” phases and/or rock fragments. The interaction of “warm” ice could be of great importance for chemical stratification and internal differentiation. Raman spectroscopy and synchrotron radiation have been used to study the bonding structure and unit cell parameters of pure Ice

VII (*Walrefen et al., 1982; Hemley et al., 1987; Pruzan et al., 1990, 1992, 1997; Fei et al., 1993; Goncharov et al., 1999; Frank et al., 2004*). However, no data exist on the effects of impurities on the bonding and unit cell parameters of solid H₂O at high pressure. To obtain more realistic data for use in planetary physics, it is important to understand the effect of impurities on H₂O at high pressure. We have chosen the NaCl–H₂O system as an analogue for more complicated “dirty” ice systems. This study measured the unit cell volumes of Ice VII formed from a 5 wt.% NaCl–H₂O solution, addressed volumetric effects of impurities on Ice VII, and documented changes in the OH stretching frequencies of Ice VII formed from a solute-rich H₂O solution.

2. Experimental theory and methods

We hypothesize that impurities can affect the properties of high-pressure H₂O polymorphs in H₂O-rich bodies and icy satellites. Data detailing the maximum concentration of these impurities are required to estimate the potential effectiveness of impurities on the thermodynamic properties over a range of pressures and temperatures. Therefore, we examined the incorporation of Na⁺ and Cl[−], in high-pressure H₂O phases from 1.0 to 30 GPa at 298 K by using a diamond anvil cell (DAC) with Raman spectroscopy and synchrotron X-ray diffraction. The use of a diamond anvil cell coupled with synchrotron X-ray radiation provides pressure–temperature–volume data for the NaCl–H₂O system at conditions relevant to those present in select H₂O-rich bodies. Our work in this simplified system establishes a new technique with which future studies may use to address additional components.

2.1. Sample preparation

Aqueous solutions were prepared to cover a range of concentrations within the NaCl–H₂O system. However, the concentrations were constrained to mol% greater than 80% H₂O to evaluate the influence of impurities on the high-pressure polymorphs of H₂O and not the influence of H₂O on high-pressure phases of NaCl. The concentration of NaCl in the aqueous solution used to form Ice VII was adjusted to ascertain the maximum concentration of NaCl in Ice VII after compression at 298 K. The dissociation of NaCl in aqueous solutions results in Na⁺ and Cl[−] being incorporated into high-pressure phases of H₂O. If diffraction lines, optical evidence, or Raman spectra indicative of NaCl are noted in addition to Ice VI or Ice VII, the maximum concentration of the impurity was interpreted to have been exceeded. We iter-

ated our starting concentrations to bracket the maximum concentration of each impurity in the ice.

Rhenium and stainless steel gaskets were used in these experiments and were pre-indented to 10–20 GPa decreasing the thickness of the gasket from 400 to 60–25 μm . Gold foil was fastened into the compressed region of the gasket to decrease the potential of reaction with the fluid and the possibility of leakage. Sample chambers of 350–100 μm diameters were drilled in the compressed regions by using an electrical discharge machine (EDM). The hole acted as the sample chamber bound on the sides by the gold-lined gasket and placed between the two diamond anvils. The H_2O aqueous solution, with dissolved NaCl, and a pressure indicator (gold for X-ray experiments and ruby for Raman spectroscopy) were loaded into the sample chamber and compressed, at room temperature, to approximately 1 GPa to seal the contents in the sample chamber. Great care was taken so that the compositions of the solutions loaded into DACs were not altered during compression. Experiment duration was varied and numerous replicate experiments were performed to determine if equilibrium had been obtained. This study used time invariance, replicate analyses and reversals as a measure of the approach to equilibrium.

2.2. X-ray diffraction

Powder X-ray diffraction experiments were conducted by using synchrotron radiation at the Advanced Photon Source, Argonne National Laboratory. The samples were contained in symmetric piston-cylinder DACs. The diamonds (type Ia, gem-quality, 0.25 carat, flawless brilliant design, 250–550 μm culet, approximately 2–3 mm in height) were mounted on tungsten carbide seats using Resbond 940 brand cement. Angle dispersive X-ray techniques were used to measure the diffraction lines of all phases present within the sample chamber. The overlap of diffraction lines for NaCl, Ice VII, and gold are minimal over the majority of the pressure range of this study. The experiments were conducted at the GSECARS 13-BM-D beamline, using monochromatic X-ray radiation and an online imaging system. The wavelength of the incident radiation was 0.3344 \AA . The diffraction lines of the sample were compared continuously to the unit cell parameters of Ice VII, NaCl, and gold during the experiment with gold being used as an internal pressure marker. Data were analyzed using the FIT2D software package (Hammersley, 1997). CeO_2 was used to calibrate the sample to detector distance, coordinates of the directed beam on the detector, and the angle and tilt of the detector. The ambient pres-

sure volume of gold and halite starting materials were compared to volumes measured using synchrotron radiation to provide another constraint on the accuracy and precision of the methods employed at the Advanced Photon Source. The unit cell parameter of gold determined from the diffraction lines was used in conjunction with a previously established *PVT* equation of state (Anderson et al., 1989). Variations in the gold unit cell volume calculated from the $\{111\}$, $\{200\}$, $\{220\}$, $\{311\}$, $\{222\}$ and $\{400\}$ diffraction lines were monitored and used to assess deviatoric stresses attributed to the non-hydrostatic environment of the diamond anvil cell (Meng et al., 1993). The uncertainty in the unit cell parameter for gold, and thus the calculated pressure, was propagated through the pressure calculation to provide a minimum pressure uncertainty.

2.3. Raman spectroscopy

Experiments using Raman spectroscopy were prepared in a fashion similar to X-ray diffraction experiments, with the noted switch of pressure indicators from gold to ruby. Small grains of ruby were dispersed throughout the sample chamber and Raman spectroscopy was used to measure the ruby R1 fluorescence line shift with increasing pressure (Mao et al., 1986). The sample and ruby grains were analyzed at intervals of approximately 1–2 GPa. The sample and ruby grains were excited by a 514.532 μm Ar laser producing inelastic Raman scattering measured by a single-stage 460 mm spectrograph with notch filters and a liquid nitrogen cooled CCD. Each measurement obtained from Raman spectroscopy indicated a Raman shift (cm^{-1}) corresponding to a frequency of molecular vibration. In addition to measuring the ruby R1 shift, the frequency change of the OH group within Ice VII was also measured. Data obtained through Raman spectroscopy was used as an additional check on the phase identification and to ascertain the O–H stretching mode frequency of the high-pressure ices over a large pressure range to gain insight into potential changes in the structure of Ice VI and VII, and Ice X formed from solute-bearing aqueous solutions.

3. Results

This study found that diamond anvil cell work on solutions with dissolved salts must be loaded quickly and brought up to pressure within 1 min of the solution load. Any evaporation of the solution will shift the solute concentration to unknown values that are higher than the target salinity. Additionally, if a sample load-

ing was attempted and not successful, the gasket needed to be removed from the assembly and cleaned extensively. The solute concentration of the solution trapped in a second attempt would most likely trap a solution of elevated and unknown concentration if another loading was attempted without removing the gasket and cleaning the sample chamber in an ultra sonic cleaner. This procedural step was only required if the first attempt at loading the cell assembly was unsuccessful, but it was an absolutely necessary procedure for second loadings.

3.1. X-ray diffraction

A NaCl–H₂O solution containing 5 wt.% (1.6 mol% NaCl) and gold (internal pressure marker) were compressed in a symmetric diamond anvil cell, so that Ice VI became the stable H₂O phase. Additional increases in pressure saw the transition from Ice VI to Ice VII at a pressure of approximately 2.4 GPa. Optical observations indicated that the sample was composed of the two phases, Ice VII and gold, whereas no additional phases were observed. Synchrotron angle dispersive X-ray diffraction data indicate that the sample diffraction lines can be indexed as either gold or Ice VII (Fig. 1). The data indicate that no separate phase of NaCl is present. These results suggest that the Ice VII formed

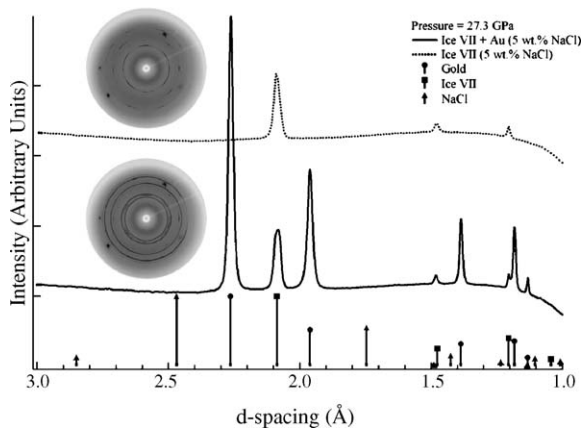


Fig. 1. The diffraction of Ice VII and gold (pressure marker) were obtained as images (inset pictures) and converted to intensity–*d*-spacing plots for analysis. The dark lines in the lower image are gold diffraction lines whereas the less intense lines (in both images) are a result of Ice VII diffraction. Diffraction patterns were generated from Ice VII only (dashed lines and uppermost image) and Ice VII + gold (solid line and lower image) sections of the sample chamber at every pressure; the presence of gold was not found to affect Ice VII diffraction. The pressure of this experiment is 27.34 ± 0.39 GPa. The diffractograms of Ice VII formed from a 5 wt.% NaCl solution displayed no evidence of halite diffraction. Hence, our working hypothesis is that Ice VII formed from a 5 wt.% solution at 298 K is undersaturated with respect to halite.

from the NaCl–H₂O solution was able to incorporate all of the Na⁺ and Cl[−] into the high-pressure ice phase. We interpret the high-pressure ice formed from a 5 wt.% NaCl–H₂O solution as lying within a one-phase field and as being undersaturated with respect to NaCl. This phase's diffraction lines are shifted systematically to lower *d*-spacing and the {200} diffraction line is of greater intensity relative to the expected diffraction lines of pure Ice VII.

Unlike the 5 wt.% NaCl–H₂O solution, compression of a 10 wt.% NaCl–H₂O solution (3.3 mol% NaCl) produces NaCl as a separate crystalline phase as indicated in Fig. 2. Additionally, as pressure is increased, NaCl diffraction lines become more pronounced in samples where the Ice VII formed from a 10 wt.% NaCl–H₂O solution. These data allow us to determine the maximum concentration of Na⁺ and Cl[−] that can be incorporated into Ice VII as 7.5 ± 2.5 wt.% or (2.4 ± 0.8) mol% NaCl. The following sections dealing with the development of an equation of state and Raman spectroscopy will concentrate on Ice VII formed from a 5 wt.% NaCl–H₂O solution.

3.2. Isothermal compression of Ice VII at 298 K

Ice VII formed from a 5 wt.% NaCl–H₂O solution was compressed at 298 K and the {110}, {200}, {210}, {220} and {310} diffraction lines of Ice VII were used to calculate its unit cell parameters

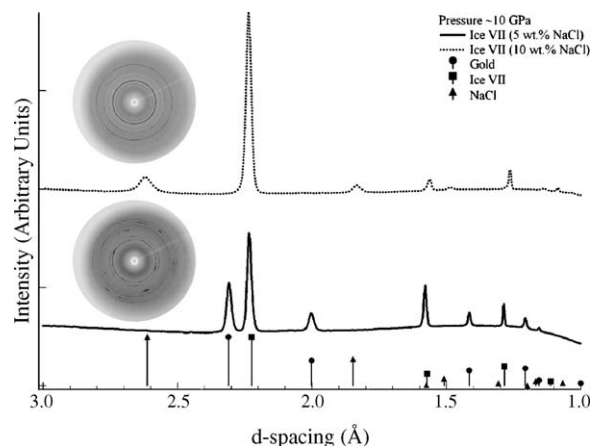


Fig. 2. The dotted-line diffraction pattern was obtained from a gold-absent area of a sample chamber containing Ice VII (formed from a 10 wt.% NaCl solution) and halite. The halite diffraction lines are also visible in the uppermost diffraction image. A comparison of the two diffractograms, both are at approximately 10 GPa, indicates that the Ice VII formed from a 10 wt.% NaCl solution (dotted line) is saturated with halite, whereas, Ice VII formed from a 5 wt.% NaCl solution (solid line) is undersaturated. We hypothesize that halite saturation in Ice VII lies between 5 and 10 wt.% NaCl at 298 K.

Table 1

Pressure and volume data for Ice VII formed from a 5 wt.% NaCl–H₂O solution at 298 K

Ice VII formed from 5 wt.% NaCl–95 wt.% H ₂ O		
Pressure (GPa)	Unit cell parameter (Å)	Volume (Å ³)
2.70 ± 0.05	3.2946 ± 0.0011	35.760 ± 0.012
2.78 ± 0.31	3.2097 ± 0.0014	35.987 ± 0.014
4.14 ± 0.16	3.2682 ± 0.0009	34.907 ± 0.010
4.25 ± 0.23	3.2076 ± 0.0010	34.973 ± 0.010
4.51 ± 0.13	3.2435 ± 0.0008	34.123 ± 0.009
4.86 ± 0.20	3.2564 ± 0.0020	34.531 ± 0.022
5.40 ± 0.24	3.2101 ± 0.0030	33.078 ± 0.031
5.83 ± 0.42	3.2060 ± 0.0021	32.953 ± 0.022
6.16 ± 0.33	3.1995 ± 0.0063	32.615 ± 0.064
6.50 ± 0.38	3.2023 ± 0.0020	32.839 ± 0.021
6.52 ± 0.39	3.2019 ± 0.0021	32.826 ± 0.022
6.55 ± 0.42	3.2018 ± 0.0022	32.823 ± 0.023
7.62 ± 0.47	3.1729 ± 0.0024	31.943 ± 0.024
7.72 ± 0.16	3.1801 ± 0.0008	32.160 ± 0.008
7.80 ± 0.41	3.1699 ± 0.0021	31.852 ± 0.021
7.85 ± 0.23	3.1780 ± 0.0012	32.097 ± 0.012
8.80 ± 0.40	3.1635 ± 0.0020	31.659 ± 0.020
9.08 ± 0.52	3.1579 ± 0.0018	31.492 ± 0.018
9.68 ± 0.29	3.1491 ± 0.0013	31.229 ± 0.013
10.47 ± 0.59	3.1266 ± 0.0028	30.564 ± 0.027
11.28 ± 0.48	3.1226 ± 0.0022	30.447 ± 0.021
11.72 ± 0.50	3.1125 ± 0.0023	30.153 ± 0.022
11.75 ± 0.40	3.1049 ± 0.0017	29.931 ± 0.016
11.83 ± 0.35	3.1055 ± 0.0016	29.950 ± 0.015
12.06 ± 0.36	3.1043 ± 0.0016	29.915 ± 0.015
12.12 ± 0.38	3.0997 ± 0.0017	29.782 ± 0.016
13.10 ± 0.55	3.0972 ± 0.0024	29.710 ± 0.023
13.29 ± 0.36	3.0909 ± 0.0016	29.529 ± 0.015
15.54 ± 0.55	3.0566 ± 0.0022	28.557 ± 0.021
15.56 ± 0.61	3.0556 ± 0.0025	28.529 ± 0.023
15.67 ± 0.59	3.0530 ± 0.0024	28.456 ± 0.022
16.31 ± 0.67	3.0418 ± 0.0027	28.144 ± 0.025
18.31 ± 0.68	3.0262 ± 0.0026	27.714 ± 0.024
21.12 ± 0.70	2.9979 ± 0.0025	26.943 ± 0.022
22.79 ± 0.77	2.9794 ± 0.0027	26.448 ± 0.024
24.61 ± 0.60	2.9693 ± 0.0066	26.096 ± 0.059
27.34 ± 0.39	2.9398 ± 0.0012	25.407 ± 0.011

Gold was used as a pressure marker and the pressure was obtained from the gold unit cell parameter. Refer to the text for a discussion of uncertainty.

where possible (Table 1). The 298 K compression data were collected up to 27 GPa and fit to a third-order Birch–Murnaghan equation of state (Birch, 1978) of the form:

$$P \text{ (GPa)} = \frac{3}{2} K_{T0} \left[\left(\frac{V_0}{V} \right)^{7/3} - \left(\frac{V_0}{V} \right)^{5/3} \right] \times \left[1 - \frac{3}{4} (4 - K'_{T0}) \left(\left(\frac{V_0}{V} \right)^{2/3} - 1 \right) \right] \quad (1)$$

where K_{T0} , K'_{T0} and V_0 are the isothermal bulk modulus, its pressure derivative and the volume at zero pressure, respectively. Ice VII is a non-quenchable phase and so its V_0 had to be calculated simultaneously with K_{T0} and K'_{T0} . Our best-fit *EOS* results give K_{T0} , K'_{T0} and V_0 values of 26.2 ± 1.4 GPa, 4.08 ± 0.18 , and $39.1 \pm 0.2 \text{ \AA}^3$, respectively (Fig. 3; Table 2). Due to the limited compression range of this study and the resultant increase in uncertainty, we also fit our data using the K'_{T0} value from Hemley et al. (1987) for pure Ice VII. We thus calculated $K_{T0} = 25.7 \pm 0.4$ GPa, $K'_{T0} = 4.15$ (fixed), and $V_0 = 39.1 \pm 0.1 \text{ \AA}^3$, which are broadly consistent with our best-fit *EOS*. The bulk modulus, 26.2 ± 1.4 GPa, of Ice VII (5 wt.% NaCl) analyzed in this study was found to be approximately 10–20% greater relative to Ice VII formed from pure H₂O.

3.3. Raman spectroscopy

Raman spectroscopic studies of pure Ice VII and Ice VII formed from a 5 wt.% NaCl–H₂O solution were performed to determine the OH stretching frequency of the respective ices (Table 3). The OH stretching frequency of Ice VII formed from pure and solute-bearing H₂O was found to vary inversely with pressure; that is, the O–H bond lengthens with increasing pressure as the O–O distance in the O–H–O unit decreases (e.g., Walrafen et al.,

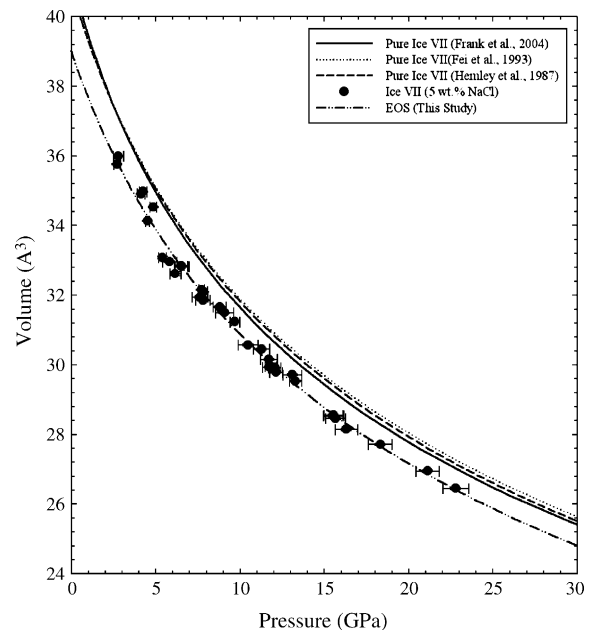


Fig. 3. The *PVT* relations of Ice VII formed from a 5 wt.% NaCl solution and pure H₂O indicate that Ice VII with Na⁺ and Cl[−] incorporated into its structure has its volume reduced by approximately 5% relative to pure H₂O Ice VII.

Table 2

Comparison of zero-pressure volume (V_0), bulk modulus (K_{T0}), and pressure derivative (K'_{T0}) for pure Ice VII (Frank et al., 2004; Hemley et al., 1987; Fei et al., 1993) to Ice VII formed from a 5 wt.% NaCl aqueous solution (this study)

	V_0 (\AA^3)	K_{T0} (GPa)	K'_{T0}
This study 5 wt.% NaCl–H ₂ O ^a	39.1 ± 0.2	26.2 ± 1.4	4.08 ± 0.18
This study 5 wt.% NaCl–H ₂ O ^b	39.1 ± 0.1	25.7 ± 0.4	4.15
Frank et al. (2004)	41.2 ± 0.1	21.3 ± 1.3	4.4 ± 0.1
Fei et al. (1993)	40.9 ± 0.7	23.9 ± 0.7	4.2 ± 0.5
Hemley et al. (1987)	40.9 ± 0.9	23.7 ± 0.9	4.15 ± 0.07

^a These values represent the best fit for the third-order Birch–Murnaghan equation of state; the Q of this fit is 0.0018.

^b This fit was obtained by setting the K'_{T0} to 4.15 (following the work of Hemley et al., 1987); the Q of this fit is 0.0024. Q is the probability that chi-squared will exceed the previously given values.

1982 and Pruzan et al., 1990 for H₂O and D₂O systems). Fig. 4 illustrates select Raman patterns for the determination of the OH stretching frequency of Ice VII formed from a 5 wt.% NaCl aqueous solution. Comparison of our data in the H₂O system to the data of Walrafen et al. (1982) and Pruzan et al. (1990) shows the three data sets are in good agreement to approximately 15 GPa (Fig. 5). The Walrafen et al. (1982) data divergence from the two other datasets at a pressure of approximately 15 GPa. The data presented in this study and Pruzan et al. (1990) follow an approximately linear trend to 27.6 GPa. The

Table 3

Pressure and $\Delta\nu_{\text{OH}}$ data for Ice VII formed from a 5 wt.% NaCl–H₂O solution and a pure H₂O solution at 298 K

Raman spectroscopic data			
Ice VII (H ₂ O)		Ice VII (5 wt.% NaCl–95 wt.% H ₂ O)	
$\Delta\nu_{\text{OH}}$ (cm ⁻¹)	Pressure (GPa)	$\Delta\nu_{\text{OH}}$ (cm ⁻¹)	Pressure (GPa)
3256	3.0 ± 0.1	3241	4.4 ± 0.1
3235	3.8 ± 0.1	3200	6.2 ± 0.1
3174	6.0 ± 0.1	3181	7.1 ± 0.1
3144	7.1 ± 0.1	3154	8.2 ± 0.3
3127	8.0 ± 0.1	3128	9.0 ± 0.1
3092	9.3 ± 0.1	3108	10.0 ± 0.1
3075	9.6 ± 0.1	3074	11.4 ± 0.2
3071	10.0 ± 0.2	3044	12.7 ± 0.2
3044	11.2 ± 0.2	3024	13.6 ± 0.3
3018	12.3 ± 0.2	2999	14.9 ± 0.1
2999	13.4 ± 0.1	2954	16.9 ± 0.3
2983	13.7 ± 0.3	2915	18.6 ± 0.2
2985	14.0 ± 0.1	2887	20.2 ± 0.3
2942	15.9 ± 0.1	2861	21.2 ± 0.1
2910	16.3 ± 0.2		
2904	17.4 ± 0.1		
2883	18.0 ± 0.3		
2884	18.3 ± 0.1		
2856	19.9 ± 0.1		
2827	20.4 ± 0.4		
2802	22.3 ± 0.2		
2671	27.6 ± 0.4		

The uncertainty in pressure was determined by analyzing the deviation in the ruby fluorescence wavelength for at least three grains located throughout the sample chamber.

best fit for the trend followed by our data is defined by the linear equation:

$$\Delta\nu_{\text{OH}} (\text{cm}^{-1}) = 3313(\pm 4) - 23.5(\pm 0.3)P (\text{GPa}) \quad (2)$$

where $\Delta\nu_{\text{OH}}$ is the relative stretching frequency of the OH bond (cm⁻¹) and P is pressure in GPa. The results for pure H₂O found in this study appear to be an accurate representation of the $\Delta\nu_{\text{OH}}$ in Ice VII as compared to the previous studies of Walrafen et al. (1982) and Pruzan et al. (1990).

The OH stretching frequency data from Ice VII formed from a 5 wt.% NaCl–H₂O solution also show an inverse relationship with pressure (Fig. 6). A best fit can be found by using a linear relationship of:

$$\Delta\nu_{\text{OH}} (\text{cm}^{-1}) = 3337(\pm 3) - 22.6(\pm 0.2)P (\text{GPa}) \quad (3)$$

The slopes of the two trends are similar and exhibit less than 4% relative difference, the largest variation between the trends is found in the y -intercept. The systematic increase in $\Delta\nu_{\text{OH}}$ reflects a shortening of the OH bond with the addition of 5 wt.% NaCl to Ice VII. The data suggest that the incorporation of Na⁺ and Cl⁻ into Ice VII does not change the interionic bonding significantly, but rather, the presence of these impurities result in an increase of $\Delta\nu_{\text{OH}}$ by approximately 1% over the pressure range of this study.

4. Discussion

4.1. Crystal chemistry of solutes in Ice VII

Our results suggest the maximum concentration of Na⁺ and Cl⁻ that can be incorporated into Ice VII is on the order of 2.4 ± 0.8 mol% NaCl (or approximately 7.5 wt.% NaCl). The body centered cubic structure of Ice VII provides large open voids in face-centered locations within the structure where impurities may be incorporated. The introduction of charged ions, Na⁺ and Cl⁻, into the structure would most likely be in these voids.

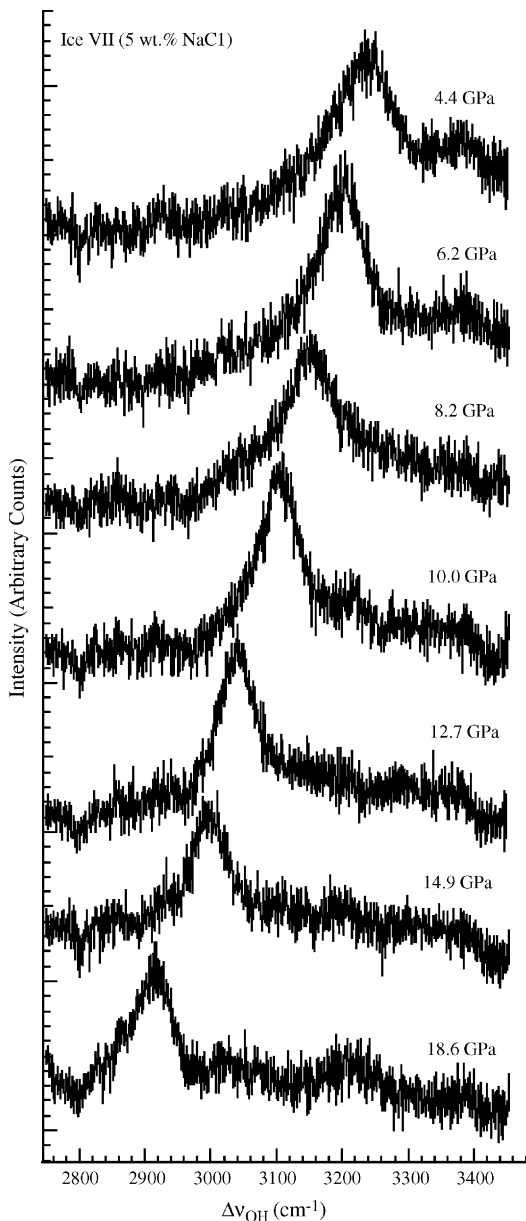


Fig. 4. This figure displays select Raman spectroscopy patterns of the $\Delta\nu_{\text{OH}}$ (cm^{-1}) of Ice VII formed from a 5 wt.% NaCl solution. The shape and intensity of the peaks do not vary measurably from those of Ice VII formed from pure H_2O .

The increase of the $\{200\}$ diffraction line of Ice VII (5 wt.% NaCl) relative to Ice VII (pure) suggests that there is an increase in the lattice nodes corresponding to some FCC crystallographic sites. The presence of charged ions in these sites should result in a rotation of the H_2O molecules to charge balance the impurities. For example, incorporation of Cl^- into the FCC site should cause the coordinating H_2O molecules to rotate

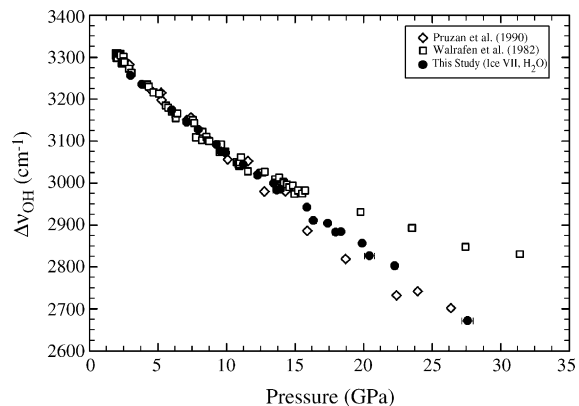


Fig. 5. A comparison of the $\Delta\nu$ values (cm^{-1}) for the OH bond in Ice VII formed from pure H_2O as a function of pressure. Our results are broadly consistent with the studies of Pruzan et al. (1990) and Walrafen et al. (1982) up to approximately 15 GPa. There is also a strong correlation between our data and the data from Pruzan et al. (1990) over the entire range of pressure.

and align the hydrogens towards the Cl^- . Raman spectroscopic data on the OH stretching frequency of Ice VII formed from a 5 wt.% NaCl aqueous solution show that there is systematic shift in $\Delta\nu_{\text{OH}}$ (cm^{-1}) to higher values as a function of pressure relative to pure Ice VII (Fig. 6). Based on the combination of the Raman and X-ray diffraction data, we hypothesized that the incorporation of Na^+ and Cl^- into Ice VII resulted in a partial ordering of the protons by interionic attractions (Na^+ with O and Cl^- with H), which resulted in a transition to an Ice X like structure, where the protons are equidistant between the oxygen atoms, at a much lower pressure. Essentially, the incorporation of Na^+ and Cl^- into Ice VII cause the H_2O molecules to “hydrate” with NaCl.

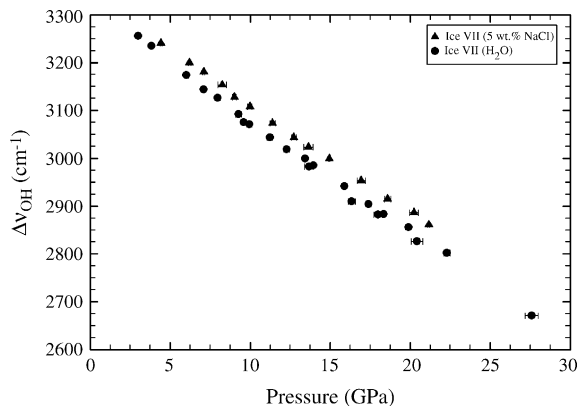


Fig. 6. A systematic elevation of $\Delta\nu_{\text{OH}}$ (cm^{-1}) as a function of pressure for Ice VII formed from a 5 wt.% NaCl solution relative to pure Ice VII was observed in this study. The increase in $\Delta\nu_{\text{OH}}$ reflects a shortening of the OH bond with the addition of 5 wt.% NaCl (as Na^+ and Cl^-) to Ice VII.

This is due to the solid solution that exists between NaCl and Ice VII and that the enthalpy of unmixing is large enough to overcome the entropy and temperature effects.

4.2. Isothermal compression of Ice VII

The properties of Ice VII at 298 K have been studied in great detail using synchrotron X-ray diffraction and Brillouin spectroscopy on both polycrystalline and single crystal samples. Hemley et al. (1987) examined Ice VII up to 128 GPa, which corresponded to a compression ratio ($V_0 - V/V_0$) of 0.13–0.58. They suggest that the zero-pressure volume, bulk modulus and its pressure derivative of Ice VII were 12.3 ± 0.3 (cm³/mol), 23.7 ± 0.9 GPa, and 4.15 ± 0.07 , respectively. Fei et al. (1993) presented Ice VII compression data ranging from 3.16 to 18.55 GPa, and, although the compression range was not as large as that of Hemley et al. (1987) or other studies, the zero-pressure volume, bulk modulus and its pressure derivative were all within the experimental uncertainty quoted by Hemley et al. (1987). Frank et al. (2004) presented data over a compression range of 0.18–0.48. They fit their data using the third-order Birch–Murnaghan equation of state and reported K_{T0} , K'_{T0} and V_0 values of 21.1 ± 1.3 GPa, 4.4 ± 0.1 , and 12.4 ± 0.1 cm³/mol, respectively; broadly consistent with the results of previous studies.

Shimizu et al. (1996) used Brillouin spectroscopy on a single crystal of Ice VII to determine the acoustic, adiabatic elastic constants and adiabatic bulk modulus. They reported a bulk modulus for Ice VII that is in good agreement with a previous X-ray study (Munro et al., 1982). X-ray diffraction data have provided the bulk of data on Ice VII with Loubeyre et al. (1999) presenting data over the largest compression range. They monitored the H₂O system up to 170 GPa and fit a Vinet form equation to their data. A zero-pressure volume, bulk modulus and its pressure derivative were calculated as 14.52 (cm³/mol), 4.26 GPa, and 7.75 . Their results were based on X-ray diffraction obtained from a single crystal. Wolanin et al. (1997) used their data and the bulk modulus taken from Shimizu et al. (1996) to calculate the zero pressure volume and the pressure derivative of the bulk modulus as 12.37 ± 0.09 and 5.4 ± 0.1 for the Birch–Murnaghan solution and 12.11 ± 0.09 and 6.2 ± 0.1 , respectively, for the Vinet solution. Although there are variations in the best-fit EOS of the previous studies, the pressure–volume data of Ice VII at 298 K are generally consistent.

Our data for Ice VII formed from a solute-bearing H₂O show a measurable depression in unit cell volume at any given pressure relative to pure Ice VII. K_{T0} , K'_{T0} , and V_0 for Ice VII at 298 K with 5 wt.% Na⁺ and

Cl[−] incorporated into its structure was determined to be 26.2 ± 1.4 , 4.08 ± 0.18 , and 39.1 ± 0.2 Å³, respectively. These results indicate that the presence of Na⁺ and Cl[−] increased the bulk modulus of the ice phase by approximately 10% while decreasing its volume (or increasing its density) by approximately 5% relative to Ice VII formed from pure H₂O at any given pressure.

The increase in the bulk modulus with the addition of NaCl is indicative of a stiffening of the Ice VII structure and a greater resistance to the effects of pressure on the unit cell volume. This is potentially important for models of ice-rich planetary bodies. For example, at 2 GPa, pure Ice VII has a volume of 37.0 Å³, but as 5 wt.% NaCl, as Na⁺ and Cl[−], is incorporated into the structure, the volume decreases to 35.5 Å³. At 10 GPa, the volume of Ice VII is 32.0 Å³, whereas, the volume of the Ice VII formed from the 5 wt.% NaCl solution is 30.8 Å³. As volume is inversely related to density, the density would be expected to increase as Na⁺ and Cl[−] are incorporated into the structure of Ice VII.

4.3. Implications for planetary physics

Data from the Galileo mission greatly increased the quality and quantity of data on the Galilean satellites and have been used extensively to produce comprehensive models on the interior of the bodies and on their formation and evolution (Anderson et al., 1996; Anderson et al., 1997; Anderson et al., 1998; Anderson et al., 2001; Kuskov and Kronrod, 2001; Sohl et al., 2002). These studies propose a wide range of models to explain the moment of inertia and density data for the Galilean satellites. The large icy satellites, with the exception of possibly Callisto, are hypothesized to contain density and chemical stratified layers (Anderson et al., 1997; Schubert et al., 1996; McKinnon, 1997; Anderson et al., 1998; Showman and Malhotra, 1999; Kuskov and Kronrod, 2001; McCord et al., 2001). Proposals for the accretion and differentiation of these bodies suggest that the ice, silicate and iron-dominated portions of the bodies interacted over a large range of pressure and temperature (Scott et al., 2002).

Magnetic field data detected during close encounters with the Galilean satellites detected perturbations in the ambient Jovian magnetic field (Kivelson et al., 1996; Schubert et al., 1996; Khurana et al., 1998; Kivelson et al., 1998). The induced magnetic fields have been interpreted as being emanated from relatively shallow portions of the icy bodies (Khurana et al., 1998; Zimmer et al., 2000; Kivelson et al., 2000; Kivelson et al., 2002) by noting the strength of the magnetic field with distance from the body. Based on the magnetic field data, and the

fact that both rock and pure H₂O phases are poor electrical conductors, a hypothesis was formulated suggesting that subsurface ocean with low to moderate salinity could be present below the outer layers of the body, but still at a relatively shallow depth. A subsurface ocean with dissolved solutes would produce the observed magnetic fields and could be responsible for some of the difficulties intrinsic in thermal modeling by affecting the thermal structure of the interior of these bodies (e.g., McKinnon, 1999; Klemaszewski and Greeley, 2001; Ruiz, 2001).

It is reasonable to assume that the subsurface fluids have interacted with the deeper ice and rock portions of the body over the course of the body's history. The extent of interaction between a subsurface ocean and a deeper rock-dominated or ice-dominated layer is unclear. Determining the phase relations and thermodynamic properties of the components within the bodies are difficult, much less trying to ascertain the pertinent equilibria needed to model the system. Few experimental studies have examined the influence of solutes on phase relations in the icy satellites (Kargel, 1991; Kargel et al., 1991; Kargel, 1992). Hogenboom et al. (1995) and Hogenboom et al. (1997) examined the MgSO₄–H₂O and ammonia–water system up to 400 MPa and noted that the presence of NH₃ lowered the solidus to 176.16 K at 0.1 MPa. Their pioneering work helped to illustrate that using experimental data from one-component systems (e.g., H₂O) in model of large icy bodies was ill advised if experimental data for more complicated and relevant systems were available. The Hogenboom et al. (1995) and Hogenboom et al. (1997) are not all-inclusive, but that data from the MgSO₄–H₂O and NH₃–H₂O systems serve as a better choice for the icy satellites than pure H₂O systems. Their study was limited to pressures that ranged from 0.1 to 400 MPa, making the application of their results to the likely high-pressure phases of H₂O within the larger icy satellites difficult. Additionally, the experimental phase relations and the thermodynamic data are sparse for multi-component systems at high pressures and more experimental data must be obtained and interpreted to advance the modeling work on the icy bodies. Our study is the first to examine the influence of impurities on the density and bonding structure of high-pressure H₂O phases.

A rudimentary calculation was completed to estimate what effect a 5% increase in density would have on the thickness of high-pressure ice layers within Callisto. The 5% increase in density was chosen based on the results presented in this study for Na⁺ and Cl[−] incorporation into Ice VII. The model calculated the thickness of the core, high-pressure ice layers (Ice VI and Ice VII), and outer ice + fluid layer that would satisfy the calcu-

lated moment of inertia and known mass for Callisto. A radius, mass, and moment of inertia (I/MR^2) for Callisto of 2.403×10^6 m, 1.077×10^{23} kg, and 0.406 were used for the calculation, respectively. The model was constrained so that the density at the core of the body was 4500 kg/m³ and the outer ice–fluid layer had a bulk density of 1200 kg/m³. We estimated the bulk density of both pure and impurity-rich Ice VI and Ice VII over the appropriate pressure and temperature range and applied the data to two separate models. The core size of Callisto was allowed to range from zero up to a maximum of 680 km; this limited range in core size was found to have only a minimal impact on the thickness of the outer ice layers. The results suggest that a 5% increase in the density of Ice VI and Ice VII results in a compaction of the high-pressure ice layer that increased the outer, low-pressure ice and fluid layer thickness by approximately 70 km. The expansion of the model outer ice and fluid layers allows for a much thicker fluid H₂O layer than thought previously; which will increase the portion of the planetary body which could potentially host life. The data presented here are limited to the NaCl–H₂O system and can be only considered as a simple analog to H₂O-rich planetary bodies. Additionally, the incorporation of impurities may also affect ice rheology (Durham and Stern, 2001; Durham et al., 1996) and could potentially inhibit convection, thus, producing measurably warmer ocean temperatures. Future experiments detailing the incorporation of other cation–anion pairs and associated compounds, such as KCl, MgSO₄ and NH₃ are needed for the next generation of models detailing the differentiation and chemical stratification of H₂O-rich bodies.

5. Conclusions

This study has shown that the maximum concentration of NaCl in Ice VII is 7.5 ± 2.5 wt.% at 298 K. Ice VII formed from a 5 wt.% NaCl–H₂O solution has a molar density that is systematically higher at any given pressure relative to the molar density of Ice VII formed from pure H₂O. The increase in the bulk modulus of Ice VII formed from a NaCl–H₂O solution relative to pure H₂O suggests that the incorporation of these impurities results in a general stiffening of the structure resulting in a greater resistance of volume to pressure increases. Raman data confirm the incorporation of Na⁺ and Cl[−] into Ice VII and suggest that the impurities cause a decrease in the OH-bond length of Ice VII. Our results suggest that ice-phases formed in a solute-rich environment or by reaction with other phases within the interior of an icy body could have a greater molar density than ice formed from pure H₂O. This phenomenon could affect the accu-

racy of current stratification models for H₂O-rich bodies such as Callisto and Europa. Our data will allow for more precise and accurate density profile and thermophysical modeling of H₂O-rich bodies.

Acknowledgements

This research was supported by the Research and Artistry Program at Northern Illinois University (MRF). CER was supported by the Intern program of The Geophysical Laboratory, Carnegie Institution of Washington during the initial phases of this project. Portions of this work were performed at GeoSoilEnviroCARS (Sector 13), Advanced Photon Source (APS), Argonne National Laboratory. GeoSoilEnviroCARS is supported by the National Science Foundation—Earth Sciences (EAR-0217473), Department of Energy—Geosciences (DE-FG02-94ER14466) and the State of Illinois. Use of the APS was supported by the U.S. Department of Energy, Basic Energy Sciences, Office of Science, under Contract No. W-31-109-Eng-38. This manuscript benefited greatly from discussions with Yingwei Fei, Russell Hemley, and Philip A. Candela on high-pressure mineral physics, thermodynamics and solid solutions. We would like to thank David Rubie and two anonymous PEPI reviewers for many helpful comments on this manuscript.

References

- Anderson, J.D., Lau, E.L., Sjogren, W.L., Schubert, G., Moore, W.B., 1996. Gravitational constraints on the internal structure of Ganymede. *Nature* 384, 541–543.
- Anderson, J.D., Lau, E.L., Sjogren, W.L., Schubert, G., Moore, W.B., 1997. Gravitational evidence for an undifferentiated Callisto. *Nature* 387, 264–266.
- Anderson, J.D., Schubert, G., Jacobson, R.A., Lau, E.L., Moore, W.B., Sjogren, W.L., 1998. Distribution of rock, metals, and ices in Callisto. *Science* 280, 1573–1576.
- Anderson, J.D., Jacobson, R.A., McElrath, T.P., Moore, W.B., Schubert, G., Thomas, P.C., 2001. Shape, mean radius, gravity field, and interior structure of Callisto. *Icarus* 153, 157–161.
- Anderson, O.L., Isaak, D.G., Yamamoto, S., 1989. Anharmonicity and the equation of state for gold. *J. Appl. Phys.* 65, 1534–1543.
- Birch, F., 1978. Finite strain isotherm and velocities for single-crystal and polycrystalline NaCl at high pressures and 300 K. *J. Geophys. Res.* A 83, 1257–1268.
- Brown, M.E., Calvin, W.M., 2000. Evidence for crystalline water and ammonia ices on Pluto's satellite charon. *Science* 287, 107–110.
- Carlson, R.W., Smythe, W., Baines, K.H., Barbini, E., Becker, K., Burns, R., Calcutt, S., Calvin, W.M., Clark, R.N., Danielson, G.E., Davies, A.G., Drossart, P., Encrenaz, T., Fanale, F.P., Granahan, J., Hansen, G., Herrera, P., Hibbitts, C., Hui, J., Irwin, P., Johnson, T.V., Kamp, L.W., Kieffer, H.H., Leader, F., Lellouch, E., Lopes-Gautier, R., Matson, D.L., McCord, T.B., Mehlman, R., Ocampo, A., Orton, G., Roos-Serote, M., Segura, M., Shirley, J., Soderblom, L., Stevenson, A., Taylor, F., Torson, J., Weir, A., Weissman, P., 1996. Near-infrared spectroscopy and spectral mapping of Jupiter and the Galilean satellites; results from Galileo's initial orbit. *Science* 274, 385–388.
- Consolmagno, G.J., Lewis, J.S., 1976. The evolution of icy satellite interiors and surfaces. *Icarus* 34 (2), 280–293.
- Datchi, F., Loubeyre, P., LeToullec, R., 2000. Extended and accurate determination of the melting curves of argon, helium, Ice (H₂O), and hydrogen (H₂). *Phys. Rev. B* 61, 6535–6546.
- Durham, W.B., Stern, L., 2001. Rheological properties of water ice—applications to the satellites of the outer planets. *Ann. Rev. Earth Planet. Sci.* 29, 295–330.
- Durham, W.B., Stern, L.A., Kirby, S.H., 1996. Rheology of water ices V and VI. *J. Geophys. Res., B, Solid Earth Planets* 101, 2989–3001.
- Fei, Y., Mao, H.K., Hemley, R.J., 1993. Thermal expansivity, bulk modulus, and melting curve of H₂O–Ice VII to 20 GPa. *J. Chem. Phys.* 99, 5369–5373.
- Frank, M.R., Fei, Y., Hu, J., 2004. Constraining the equation of state of fluid H₂O to 80 GPa using the melting curve, bulk modulus and thermal expansivity of Ice VII. *Geochim. Cosmochim. Acta* 68 (13), 2781–2790.
- Goncharov, A.F., Struzhkin, V.V., Mao, H.K., Hemley, R.J., 1999. Raman spectroscopy of dense H₂O and the transition to symmetric hydrogen bonds. *Phys. Rev. Lett.* 83, 1998–2001.
- Greeley, R., Figueredo, P.H., Williams, D.A., Chuang, F.C., Klemaszewski, J.E., Kadel, S.D., Prockter, L.M., Pappalardo, R.T., Head III, J.W., Collins, G.C., Spaun, N.A., Sullivan, R.J., Moore, J.M., Senske, D.A., Tufts, B.R., Johnson, T.V., Belton, M.J.S., Tanaka, K.L., 2000. Geologic mapping of Europa. *J. Geophys. Res.* E, Planets 105, 22559–22578.
- Greeley, R., Klemaszewski, J.E., Wagner, R., 2000b. Galileo views of the geology of Callisto. *Planet. Space Sci.* 48, 829–853.
- Hammersley, A.P., 1997. FIT2D: An Introduction and Overview. ESRF Internal Report ESRF97HA02T.
- Head, J.W., Pappalardo, R., Collins, G., Belton, M.J.S., Giese, B., Wagner, R., Breneman, H., Spaun, N., Nixon, B., Neukum, G., Moore, J., 2002. Evidence for Europa-like tectonic resurfacing styles on Ganymede. *Geophys. Res. Lett.* 29, 1–4.
- Hemley, R.J., Jephcoat, A.P., Mao, H.K., Zha, C.S., Finger, L.W., Cox, D.E., 1987. Static compression of H₂O–Ice to 128 GPa (1.28 Mbar). *Nature* 330, 737–740.
- Hogenboom, D.L., Kargel, J.S., Ganasan, J.P., Lee, L., 1995. Magnesium sulfate–water to 400 MPa using a novel piezometer: densities, phase equilibria, and planetological implications. *Icarus* 115, 258–277.
- Hogenboom, D.L., Kargel, J.S., Consolmagno, G.J., Holden, T.C., Lee, L., Buyounouski, M., 1997. The ammonia–water system and the chemical differentiation of the icy satellites. *Icarus* 128, 171–180.
- Hubbard, W.B., Marley, M.S., 1989. Optimized Jupiter, Saturn, and Uranus interior models. *Icarus* 78, 102–118.
- Kargel, J.S., 1991. Brine volcanism and the interior structures of asteroids and satellites. *Icarus* 94, 368–390.
- Kargel, J.S., 1992. Ammonia–water volcanism on icy satellites: phase relations at 1 atmosphere. *Icarus* 100, 556–574.
- Kargel, J.S., Croft, S.K., Lunine, J.I., Lewis, J.S., 1991. Rheological properties of ammonia–water liquids and crystal–liquid slurries: planetological applications. *Icarus* 89, 93–112.
- Khurana, K.K., Kivelson, M.G., Stevenson, D.J., Schubert, G., Russell, C.T., Walker, R.J., Polansky, C., 1998. Induced magnetic fields as evidence for subsurface oceans in Europa and Callisto. *Nature* 395, 777–780.

- Kivelson, M.G., Khurana, K.K., Russell, C.T., Walker, R.J., Warnecke, J., Coroniti, F.V., Polansky, C., Southwood, D.J., Schubert, G., 1996. Discovery of Ganymede's magnetic field by the Galileo spacecraft. *Nature* 384, 537–541.
- Kivelson, M.G., Khurana, K.K., Russell, C.T., Volwerk, M., Walker, R.J., Zimmer, C., 2000. Galileo magnetometer measurements: a stronger case for a subsurface ocean at Europa. *Science* 289, 1340–1343.
- Kivelson, M.G., Khurana, K.K., Volwerk, M., 2002. The permanent and inductive magnetic moments of Ganymede. *Icarus* 157, 507–522.
- Kivelson, M.G., Warnecke, J., Bennett, L., Joy, S., Khurana, K.K., Linker, J.A., Russell, C.T., Walker, R.J., Polansky, C., 1998. Ganymede's magnetosphere: magnetometer overview. *J. Geophys. Res.* 103, 19963–19972.
- Klemaszewski, J.E., Greeley, R., 2001. Geological evidence for an ocean on Callisto. *Lunar Planet. Sci.* XXXII, 1818.
- Kuskov, O.L., Kronrod, V.A., 2001. Core sizes and internal structure of Earth's and Jupiter's satellites. *Icarus* 151, 204–227.
- Loubeyre, P., LeToullec, R., Wolanin, E., Hanfland, M., Häusermann, D., 1999. Modulated phases and proton centering in ice observed by X-ray diffraction up to 170 GPa. *Nature* 397, 503–506.
- Mao, H.K., Xu, J., Bell, P.M., 1986. Calibration of the ruby pressure gauge to 800 kbar under quasi-hydrostatic conditions. *J. Geophys. Res.* B 91 (5), 4673–4676.
- McCord, T.B., Hansen, G.B., Fanale, F.P., Carlson, R.W., Matson, D.L., Johnson, T.V., Smythe, W.D., Crowley, J.K., Martin, P.D., Ocampo, A., Hibbitts, C.A., Granahan, J.C., 1998. Salts on Europa's surface detected by Galileo's near infrared mapping spectrometer. *Science* 280, 1242–1245.
- McCord, T.B., Hansen, G.B., Hibbitts, C.A., 2001. Hydrated salt minerals on Ganymede's surface: evidence of an ocean below. *Science* 292, 1523–1525.
- McKinnon, W.B., 1997. Mystery of Callisto: is it undifferentiated? *Icarus* 130, 540–543.
- McKinnon, W.B., 1999. Convective instability in Europa's floating ice shell. *Geophys. Res. Lett.* 26, 951–954.
- Meng, Y., Weidner, D.J., Fei, Y., 1993. Deviatoric stress in a quasi-hydrostatic diamond anvil cell: effect on the volume-based pressure calibration. *Geophys. Res. Lett.* 20, 1147–1150.
- Mueller, S., McKinnon, W.B., 1988. Three layered models of Ganymede and Callisto; compositions, structures, and aspects of evolution. *Icarus* 76, 437–464.
- Munro, R.G., Block, S., Mauer, F.A., Piermarini, G., 1982. Isothermal equations of state for H₂O-VII and D₂O-VII. *J. Appl. Phys.* 53, 6174–6178.
- Nellis, W.J., Hamilton, D.C., Holmes, N.C., Radosky, H.B., Rhee, F.H., Mitchell, A.C., Nicol, M., 1988. The nature of the interior of Uranus based on studies of planetary ices at high dynamic pressure. *Science* 240, 779–781.
- Pruzan, P., Chervin, J.C., Canny, B., 1992. Determination of the D₂O Ice VII–VIII transition line by Raman scattering up to 51 GPa. *J. Chem. Phys.* 97, 718–721.
- Pruzan, P., Chervin, J.C., Gauthier, M., 1990. Raman spectroscopy investigation of Ice VII and deuterated Ice VII to 40 GPa Disorder in Ice VII. *Europhys. Lett.* 13, 81–87.
- Pruzan, P., Wolanin, E., Gauthier, M., Chervin, J.C., Canny, B., 1997. Raman scattering and X-ray diffraction of ice in the megabar range occurrence of symmetric disordered solid above 62 GPa. *J. Phys. Chem.* 101, 6230–6233.
- Ruiz, J., 2001. The stability against freezing of an internal liquid–water ocean in Callisto. *Nature* 412, 409–411.
- Schenk, P.M., McKinnon, W.B., Gwynn, D., Moore, J.M., 2001. Flooding of Ganymede's bright, resurfaced terrains by low-viscosity water–ice lavas. *Nature* 410, 57–60.
- Schubert, G., Zhang, K., Kivelson, M.G., Anderson, J.D., 1996. The magnetic field and internal structure of Ganymede. *Nature* 384 (6609), 544–545.
- Scott, H.P., Williams, Q., Ryerson, F.J., 2002. Experimental constraints on the chemical evolution of icy satellites. *Earth Planet. Sci. Lett.* 203, 399–412.
- Shimizu, H., Nabetani, T., Nishiba, T., Sasaki, S., 1996. High-pressure elastic properties of the VI and VII phases of ice in dense H₂O and D₂O. *Phys. Rev. B* 53, 6107–6110.
- Showman, A.P., Malhotra, R., 1999. Tidal evolution into the Laplace resonance and the resurfacing of Ganymede. *Icarus* 127, 367–383.
- Sohl, F., Spohn, T., Breuer, D., Nagel, K., 2002. Implications from Galileo observations on the interior structure and chemistry of the Galilean satellites. *Icarus* 157, 104–119.
- Spohn, T., Schubert, G., 2003. Oceans in the icy Galilean satellites of Jupiter? *Icarus* 161, 456–467.
- Walrafen, G.E., Abebe, M., Mauer, F.A., Block, S., Piermarini, G.J., Munro, R., 1982. Raman and X-ray investigations of Ice VII to 36.0 GPa. *J. Chem. Phys.* 77 (4), 2166–2174.
- Wolanin, E., Pruzan, P., Chervin, J.C., Canny, B., Gauthier, M., Häusermann, D., Hanfland, M., 1997. Equation of state of Ice VII up to 106 GPa. *Phys. Rev. B* 56, 5781–5785.
- Zimmer, C., Khurana, K.K., Kivelson, M.G., 2000. Subsurface oceans on Europa and Callisto; constraints from Galileo magnetometer observations. *Icarus* 147, 329–347.